Chapter 2
Cerebral White Matter Segmentation using Probabilistic Graph Cut Algorithm

Mainak Sen, Ashish K. Rudra, Ananda S. Chowdhury, Ahmed Elnakib, and Ayman El-Baz

Abstract Accurate and efficient computer-assisted brain image segmentation methods are of great interest to both scientific and clinical researchers of the human central neural system. Cerebral white matter segmentation from Magnetic Resonance Imaging (MRI) data of brain remains a challenging problem due to a combination of several factors: noise and imaging artifacts, partial volume effects, intrinsic tissue variation due to neurodevelopment and neuropathologies, and the highly convoluted geometry of the cortex. We propose here a probabilistic variation of the traditional graph cut algorithm (IEEE international conference on computer vision, pp 105–112) with an improved parameter selection mechanism for the energy function, to be optimized in a graph cut problem. In addition, we use a simple yet effective shape prior in form of a series of ellipses to increase the computational efficiency of the proposed algorithm and improve the quality of the segmentation by modeling the contours of the human skull in various 2D slices of the sequence. Qualitative as well as quantitative segmentation results on T1-weighted MRI input, for both 2D and 3D cases are included. These results indicate that the proposed probabilistic graph cut algorithm outperforms some of the state-of-the art segmentation algorithms like the traditional graph cut (IEEE international conference on computer vision, pp 105–112) and the expectation maximization segmentation (IEEE Trans Med Imaging 20(8):677–688, 2001).

2.1 Introduction

Cerebral white matter segmentation has always been a challenging task for a computer assisted diagnosis system. The problem is of interest for researchers in computer vision and biomedical imaging as well as for neurologists and neurosurgeons. The segmentation problem becomes very difficult due to a combination of several factors

---

A.S. Chowdhury (✉)
Department of Electronics and Telecommunication Engineering, Jadavpur University, Calcutta 700032, India
e-mail: ananda.chowdhury@gmail.com

A. El-Baz et al. (eds.), *Multi Modality State-of-the-Art Medical Image Segmentation and Registration Methodologies*, DOI 10.1007/978-1-4419-8204-9_2,

like (a) noise and imaging artifacts, (b) partial volume effects, (c) intrinsic tissue variation due to neurodevelopment and neuropathologies, and (d) the highly convoluted geometry of the cortex. So, this problem poses great challenge to the computer vision community. In addition to the technical challenges, the problem has a lot of clinical significance, e.g., it helps us in the understanding of brain disorders like autism [1]. Furthermore, study of abnormalities and lesions in the white matter is extremely helpful for the study of multiple sclerosis, Alzheimer's disease [2], and cognitive defects in elderly subjects [3].

Graph cuts are applied over the last few years to accurately solve complex segmentation problems [4–8]. The main advantage of graph cuts is that they yield a globally optimal segmentation which can potentially overcome the problems of oversegmentation and undersegmentation. However, the success of the graph cut algorithm depends on the variation in the capacities of different edges in the graph, which in turn depends on existing contrast in the image. T1-weighted input MRI images for our problem exhibit significant low contrast and are hence are not particularly amenable to graph cut as prescribed by Boykov and Jolly [4].

A 2D slice from a T1-weighted MRI input is shown in Fig. 2.1. Note that there is pronounced low contrast between our target object, i.e., the cerebral white matter and the surrounding brain structures. One such region is indicated by a red rectangle. For better illustration, this region is zoomed in Fig. 2.2. To understand the distribution of the intensity levels (among the pixels), we present a histogram of the above region in Fig. 2.3. The histogram does not show significant variations among the intensity levels. Therefore, it becomes evident that the cerebral white matter and the neighboring structures have quite similar intensity profiles and do not exhibit high contrast. Thus it becomes necessary to modify the graph cut algorithm in [4] to have accurate segmentation results. In this work, we propose a probabilistic version of

Fig. 2.1 A T1-weighted MRI input data with the rectangle (in *red*) indicates a typical low-contrast region containing a part of cerebral white matter

Fig. 2.2 A zoomed view of the selected area in Fig. 2.1

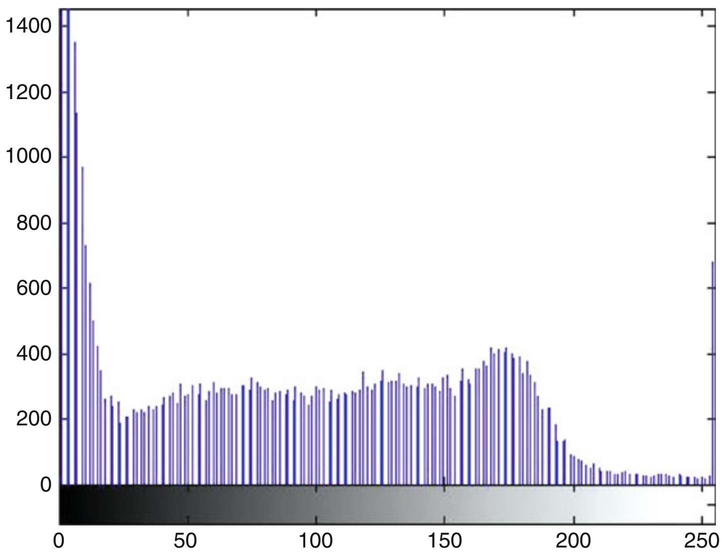

Fig. 2.3 Histogram of the selected area in Fig. **2.1**

the graph cut algorithm, described in [4] by modifying the edge capacity functions according to the probabilities of voxels to belong to different segmentation classes.

The Expectation Maximization Segmentation (EMS) algorithm proposed by Leemput et al. [9] is one important statistical method, which has been extensively used as a tissue classifier for brain MRI. In order to show the strength of our method, we have compared our 3D segmentation results with [4, 9]. An earlier version of this work, where we focused on 2D segmentation and restricted our comparison with [4], appears in [10].

The rest of the chapter is organized in the following manner: in Sect. 2.2, we present the literature review and highlight our contributions. In Sect. 2.3, we describe various components of our proposed technique, namely, the probabilistic graph cut algorithm, the variation of the weighting parameter in the energy function of the graph cut and the imposition of the shape prior. In Sect. 2.4, we discuss the experimental results for both 2D and 3D segmentation. Finally, in Sect. 2.5, we summarize and conclude the work.

2.2 Literature Review

Popular computer vision techniques for extracting a brain structure from the MRI data can be grouped into three broad categories, namely, (a) *statistical models*-based segmentation, (b) *atlas*-based segmentation, and (c) *deformable models*-based segmentation. The statistical approaches [9, 11–13] suffer from the fact that the tails of the distributions of the brain tissues (e.g., white matter, gray matter), which are modeled as a mixture of well-known distributions, are always overlapped. Thus, it becomes quite difficult to find thresholds that separate them accurately. Success of atlas-based methods [11, 12, 14] depends heavily on the high accuracy of registration between the atlas brain and the unsegmented brain, which may be hard to obtain in many cases. The main drawbacks of the deformable models [15–17] include slow speed, strong sensitivity to initialization, and incomplete segmentation in case of complicated object boundary with concavities. Graph cuts [4–8] have been applied to medical image segmentation problems including structure detections in the human brain [18].

To overcome the limitations of the various prevalent methods, we propose a probabilistic graph cut algorithm with an improved parameter selection strategy in conjunction with a simple shape prior to segment the cerebral white matter. The probabilistic graph cut algorithm effectively handles low contrast between the cerebral white matter and the surrounding anatomical structures in the MRI data. Note that the choice of the weighting parameter for the data and the smoothness terms in the energy function of the graph cut algorithm affects the segmentation performance [19]. An improved parameter selection procedure for each individual voxel is, based on the probabilities of its surrounding voxels to belong to the object class and the background class, is suggested. We further employ a simple yet effective shape prior in form of a series of ellipses to model the human skull in individual 2D slices constituting the input sequence. In sharp contrast to the methods described in [20–22], where the shape constraints are added in form of additional terms in the energy function, we use the shape constraint to generate a subgraph by pruning a significant part of the 3D graph (constructed from the input). The proposed algorithm is applied on the newly formed subgraph. So, three major contributions are (a) proposition of a probabilistic graph cut algorithm, (b) introduction of an improved parameter selection strategy for the energy function of the probabilistic graph cut algorithm and (c) the manner in which a geometric shape prior is imposed to improve computational efficiency as well as accuracy of segmentation.

2.3 Methods

Since our probabilistic graph cut method is developed on the framework of the graph cut algorithm proposed by Boykov and Jolly [4], some of its salient features are included. We will henceforth refer this algorithm as the traditional graph cut. In traditional graph cut, an user marks some pixels as being part of the object of interest, and some pixels as lying outside the object, *i.e.*, within the background. The segmentation is governed by the following criteria:

1. Each pixel inside the object is given a value according to whether its intensity matches the object's appearance model; low values represent better matches.
2. Each pixel in the background is given a value according to whether its intensity matches the background's appearance model; low values represent better matches.
3. A pair of adjacent pixels, where one is inside the object and the other is outside, is given a value according to whether the two pixels have similar intensities; low values correspond to contrasting intensities (i.e., to an edge).

Given these criteria, the goal is to design an algorithm that can find an optimal segmentation. The edge weights in this graph cut can be formulated such that a binary partitioning derived from the solution of the min-cut/max-flow algorithm minimizes certain energy function. As mentioned earlier, success of the graph cut algorithm depends on correct identification of inexpensive edges. Thus, coining of a proper energy function to capture the variations in the capacities of the edges becomes the most essential step. In the present problem, the existing intensity distribution is not particularly amenable to a correct minimum cut, which thus leads to an improper segmentation. Therefore, some probabilistic adaptation of the standard graph cut is proposed.

We first discuss the construction of the graph from the input sequence. The input MRI sequence is modeled as a weighted undirected 3D graph $G = G(V, E)$. Let X denote the set of all voxels. Each voxel $x \in X$ is a node/vertex in G. In addition, two special terminal nodes, called the "source" s and the "sink" t, are considered [23]. There are two types of edges/links in the present network, namely, the t-links (T) and the n-links (N). The t-links connect all the individual voxels x to the source node s and the sink node t. A neighborhood set $\mathrm{Ne}(x)$ is assumed for each node x. Here, we have used the 26-neighborhood, *i.e.*, $|\mathrm{Ne}(x)| = 26$. The n-links are constructed between each voxel x and its neighboring voxels y, where, $y \in \mathrm{Ne}(x)$. Therefore, we have $V = X \cup s \cup t$ and $E = T \cup N$. Note that for 2D segmentation from a single slice, a weighted undirected 2D graph is constructed. An eight-neighborhood is used in such case.

2.3.1 Probabilistic Graph Cut

Here, we describe our probabilistic graph cut algorithm. Let A define a segmentation, i.e., classification of all voxels into either "object" or "background". Then, following [4], we can write the energy function to be minimized via graph cut over the binary variable $\delta(A)$ (where $\delta(A) = 1$ when $A =$ object and $\delta(A) = 0$ when $A =$ background) as:

$$E(A) = B(A) + \lambda R(A) \tag{2.1}$$

where $B(A)$ and $R(A)$ respectively denote the smoothness term/boundary properties of segmentation A and the data term/region properties of segmentation A. Mathematical expressions for these two terms are given below:

$$B(A) = \sum_{\substack{x \in X \\ y \in \mathrm{Ne}(x)}} B_{\{x,y\}} \tag{2.2}$$

$$R(A) = \sum_{x \in X} R_x(A_x) \tag{2.3}$$

Let O, B, and I_x be the histogram of the object seeds, histogram of the background seeds, and intensity of any voxel x respectively. Further, let $\Pr(I_x|O)$ and $\Pr(I_x|B)$ denote the probability of a certain voxel x to belong to the class "object" (*i.e.*, white matter) and to the class "background" (*i.e.*, everything else in the image) respectively. We next define $B_{\{x,\ y\}}$, R_x(object), and R_x(background) in the following equations:

$$B_{\{x,y\}} = K_{\{x,y\}} \exp\left(\frac{-(I_x - I_y)^2}{2\sigma^2}\right) * \frac{1}{d(x,y)} \tag{2.4}$$

$$R_x(\text{object}) = -K_x^{\text{o}} \ln(\Pr(I_x|O)) \tag{2.5}$$

$$R_x(\text{background}) = -K_x^{\text{b}} \ln(\Pr(I_x|B)) \tag{2.6}$$

The term $d(x, y)$ denotes distance between two voxels x and y. The three terms $K_{\{x,y\}}$, $K_x^{\text{o}}, K_x^{\text{b}}$ appearing respectively in (2.4)–(2.6) are evaluated within the probabilistic graph cut algorithm.

Algorithm: Probabilistic Graph Cut
Step 1: Evaluation of $K_{\{x,y\}}$ – Compare the probabilities of any two voxels $x \in X$ and $y \in \mathrm{Ne}(x)$ to belong to the same segmentation class using the terms $\Pr(I_x|O)$, $\Pr(I_x|B)$, $\Pr(I_y|O)$, and $\Pr(I_y|B)$. If both x and y have higher probabilities to belong to the same class, assign K_1 to $K_{\{x,y\}}$. Otherwise, assign K_2 to $K_{\{x,y\}}$.
Step 2: Evaluation of K_x^{o} *and* K_x^{b} – Compare the probability of a single voxel p to belong to the segmentation class "object" or "background" using the terms $\Pr(I_x|O)$ and $\Pr(I_x/B)$. If x has a higher probability to belong to the "object" class, assign K_1 to K_x^{o} and K_2 to K_x^{b}. Otherwise, assign K_2 to K_x^{o} and K_1 to K_x^{b}.
Step 3: Apply probabilistic graph cut using (2.2)–(2.6).

In a standard graph cut algorithm, we do not consider any variation of the above three terms. Here, we define all of them within a probabilistic framework. Note that the nature of the energy function, as defined in (2.1) still remains convex, in spite of the probabilistic modifications. Thus, we can clearly apply the max-flow min-cut algorithm to find a global minimum of this energy function, which corresponds to the optimal segmentation [24]. In the next subsection, we illustrate the comparative performances of the proposed probabilistic graph cut algorithm and the traditional graph cut algorithm on a synthetic image. The value of λ in (2.1) is modified according to the technique described in the Sect. 2.3.3. There exists a lower limit of the ratio (K_1/K_2), which depends on the contrast of the image. For all values of this ratio above the lower limit, the accuracy of the segmented output remains almost constant.

2.3.2 Probabilistic Graph Cut vs. Traditional Graph Cut

In this section, we show how the proposed probabilistic graph cut algorithm achieves a better segmentation with respect to the traditional graph cut with the help of a small synthetic image containing only four pixels.

Figure 2.4 shows a low-contrast image with just four pixels, (S, Q, P, and T) having intensities I_p, I_q, I_s, and I_t respectively. Let us assume, without any loss of generality, that the right half of the image (*i.e.*, the pixels Q and T) is our region of interest (ROI). In other words, our objective is to segment these 2 pixels from the set of 4 pixels. The contrast difference between the ROI pixel set (Q, T) and foreground pixel set (S, P) is extremely low.

2.3.2.1 Segmentation using Traditional Graph Cut

We form the graph (G) from the synthetic image using the capacity functions of the traditional graph cut [4]. The four pixels (S, P, Q, and T) are the nodes of the graph constructed from the image. To find the minimum cut [23], we consider node S and node T as the source and the sink respectively without any loss of generality. As the intensity difference between the pixel P and Q is very low, the *N*-link capacity formed between them will be extremely high. Let us introduce the following symbols:
$C1$ = capacity of the T-link formed between source(S) and pixel P
$C3$ = capacity of the T-link formed between source(S) and pixel Q

Fig. 2.4 A synthetic low-contrast image with four pixels S, Q, P, and T

$C1 - X$ = capacity of the T-link formed between sink (T) and pixel P (where $X > 0$)
$C3 + Y$ = capacity of the T-link formed between sink (T) and pixel Q (where $Y > 0$)
$C2$ = capacity of the N-link formed between pixel P and pixel Q

In Fig. 2.5a, $C2$ (the capacity of the edge between P and Q) is very high and the value of X and Y is quite low due to the low contrast of the image. Now, when we calculate the maximum flow, the flow through the augmenting path 1 (S → P → T) and path 2 (S → Q → T) will be as shown in Fig. 2.5b. Now, in the case of augmenting path 3 (S → P → Q → T), the excess capacities in the edges (top to bottom respectively) are X, $C2$, and Y. As, $C2$ is greater than X and Y, we have only three cases.

Case I. $X < Y$: In this case, we can send only X units of flow along the augmenting path 3. The updated residual graph is shown in Fig. 2.6a.

Here, the maximum amount flow that can be augmented from source(S) to sink (T) is ($C1 + C3$). Figure 2.6b shows the minimum cut, which is equal to the maximum flow in the graph. We can see that it is a case of oversegmentation.

Case II. $X >$ Y: Under this condition, the maximum amount of flow we can send down this augmenting path is Y. Here, total flow is ($C1 + C3 - X + Y$). The modified flow is shown in Fig. 2.7a and the solid curved line in Fig. 2.7b shows

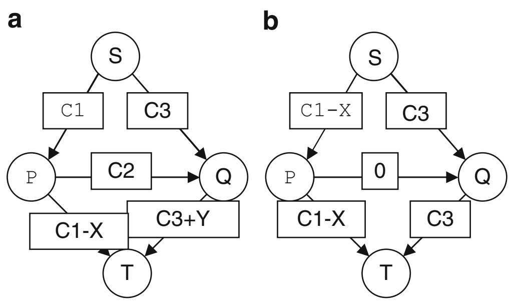

Fig. 2.5 (**a**) Graph constructed from the low-contrast image, (**b**) Flow augmented along the paths in the graph

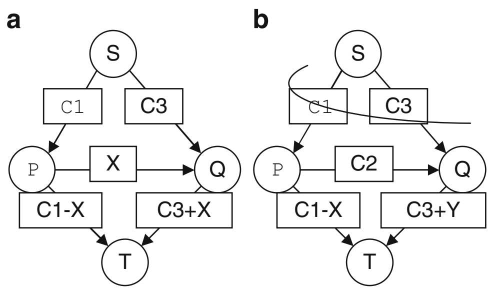

Fig. 2.6 (**a**) Updated flows along the edges after augmenting flow along the path 3 for $X < Y$; (**b**) The *solid curved line* shows the minimum cut in the graph

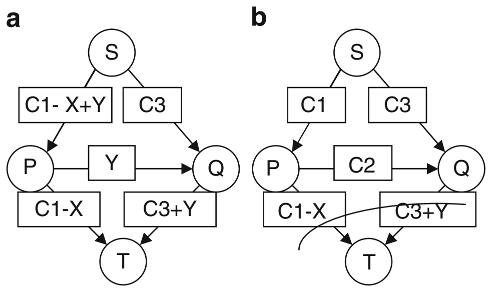

Fig. 2.7 (**a**) Updated flows along the edges after augmenting flow along the path 3 for $X > Y$; (**b**) The *solid curved line* shows the minimum cut in the graph

the minimum cut. In this case, we get an undersegmented output by applying the traditional graph cut algorithm.

Case III. $X = Y$: In this case we will get any of the two segmented outputs, obtained in the previous two cases.

So, this flow augmentation based analysis using the maxflow-mincut algorithm [23] shows that for a very low-contrast image, the traditional graph cut segmentation can not produce accurate results.

2.3.2.2 Segmentation Using Probabilistic Graph Cut

Now, we again form the graph (G) from the Fig. 2.4 incorporating our probabilistic modification in the edge capacities of the traditional graph cut algorithm. For simplicity, we take the probabilistic scaling functions as mentioned earlier, *i.e.*, $K1 = K$ and $K2 = 1$. Alternatively, we can say, K is the ratio of the two scaling functions K1 and K2.

Figure 2.3a shows the residual graph constructed from the low-contrast image. To calculate the maximum flow in G, we consider only two augmenting paths: path 1 which is S $\rightarrow$ P $\rightarrow$ T and path 2 which is S $\rightarrow$ Q $\rightarrow$ T. These two paths are shown in Fig. 2.8b, Now, in the case of path 3 which is S $\rightarrow$ P $\rightarrow$ Q $\rightarrow$ T, the excess capacities of the three edges are $(K - 1)*C1 + X$, $C2$ and $(K - 1)*C3 + K*Y$ from source to sink respectively. Now, if we chose the value of K such that it satisfies the two following conditions:

$$(K - 1)C1 + X \geq C2 \tag{2.7a}$$

$$(K - 1)C3 + KY \geq C2 \tag{2.7b}$$

then, the maximum flow through the augmenting path 3 will be $C2$. The updated flows in the graph are shown in Fig. 2.9a.

Here, the total flow is $C1 - X + C2 + C3$ and the mincut is shown in the Fig. 2.9b. In this case, we see that the segmented output is the pixel set (Q, T)

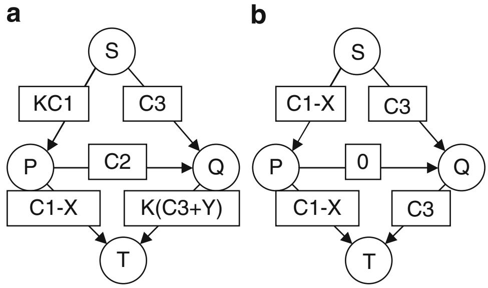

Fig. 2.8 (**a**) Graph (G); (**b**) Flows along the edges after augmenting flow along path 1 and path 2

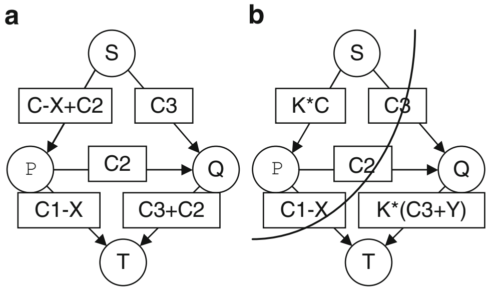

Fig. 2.9 (**a**) Augmented flow along the path 3 and the updated flows in the graph; (**b**) the *solid curved line* showing the minimum cut in the graph

which is our desired region of interest (ROI). So, we can conclude that probabilistic graph cut produces more accurate segmentation than the traditional graph cut when the input image is of low contrast.

In the previous section, we have established the criteria (see (2.7a) and (2.7b)) for K, which need to be satisfied to get the desired segmentation results. We now derive a lower limit of K, say K_L, by rewriting the eqs.(2.7a) and (2.7b). Thus, we get:

$$K \geq \frac{(C2 + (C1 - X))}{C1} \tag{2.7c}$$

$$K \geq \frac{C2 + C3}{C3 + Y} \tag{2.7d}$$

From (2.7c) and (2.7d), we can write $K_L = \max\left((C2 + (C1 - X))/C1, (C2 + C3)/(C3 + Y)\right)$. So, the value of K_L depends upon the edge capacities. Note that the capacities $C1$,$(C1 - X)$ and $C3$,$(C3 + Y)$ depend on $\Pr(I_p/O)$, $\Pr(I_p/B)$, $\Pr(I_q/O)$, and $\Pr(I_q/B)$, and $C2$ depends on $(I_p - I_q)$ or the contrast of the image according to (2.4)–(2.6). In our algorithm, we use the probability functions to formulate the edge capacities weighted by $K1$ or $K2$. Then, for a given image, the K_L essentially depends on the contrast of the image.

2.3.3 Parameter Selection Strategy

The parameter λ determines the relative importance of the smoothness term and the data term in a graph cut-based segmentation framework (see (2.1)). Proper choice of this parameter largely influences the quality of the segmented output [4, 19]. In particular, large values of λ result in a nonsmooth boundary thereby leading to oversegmentation. On the other hand, small values of λ make the boundary too smooth causing undersegmentation. Thus selecting a correct λ, which would cause neither oversegmentation nor undersegmentation, remains a fundamental problem. Significant user interaction may be necessary at many cases to obtain optimal segmentation. In order to circumvent the above problem, Peng and Veksler [19] developed an automatic parameter selections strategy with a combination of different image features using AdaBoost. However, the above method involves many steps like feature extraction, feature normalization, and training the Adaboost classifier and hence potentially requires significantly more time for completion compared to that of the standard graph cut. In this work, we have undertaken a purely probabilistic strategy for modulating the relative importance of the data term and the smoothness term, based on the location of a particular voxel in the image. The proposed method, unlike [19] is quite fast and has very similar execution time as that of the standard graph cut.

Instead of assigning a single value of λ to all the voxels, we estimate a separate value of λ_x for each individual voxel x. The value of λ_x depends on the location of the voxel x. If a voxel lies well within the foreground or the background region, the smoothness term gets more importance. In such cases, a voxel is typically surrounded by voxels whose probabilities to belong to any of the segmentation class are considerably higher than the other class. Consequently, we make the contribution of the smoothness term high by setting a lower value of λ_x. In contrast, if a voxel is close to the boundary, then we should give more importance to the data term. This is accomplished by setting a higher value of λ_x. Let A_y be the set of neighbors of any voxel x for which $\Pr(I_y|O) > \Pr(I_y|B)$. Similarly, let B_y be the set of neighbors of any voxel x for which $\Pr(I_y|B) > \Pr(I_y|O)$. Then, we set the value of λ_x using the following equation:

$$\lambda_x = \lambda_{\max} \exp(-((S_{\mathrm{A}} - S_{\mathrm{B}})/D)^2) \tag{2.9}$$

Expressions for S_{A}, S_{B}, and D are given below:

$$S_{\mathrm{A}} = \sum_{i=1}^{|A_y|} \Pr(Iy|O)/d(x, y_i) \tag{2.10}$$

$$S_{\mathrm{B}} = \sum_{i=1}^{|B_y|} \Pr(Iy|B)/d(x, y_i) \tag{2.11}$$

$$D = \sum_{i=1}^{|\mathrm{Ne}(x)|} (1/d(x, y_i)) \tag{2.12}$$

In (2.10), S_A is used to denote the total distance-weighted probability of the neighboring voxels in the set A_y to belong to the class "object". Likewise, in (2.11), S_B is used to denote the total distance-weighted probability of the neighboring voxels in the set B_y to belong to the class "background". The term D in (2.12) is used as the normalizing factor. The value of λ_{max} is experimentally determined along the lines of [19]. When a voxel is well within the object region, we have $S_A \gg S_B$. Similarly, when a voxel is well within the background region, we have $S_B \gg S_A$. In both these cases, following (2.11), we get: $\lambda_x \ll \lambda_{max}$. Consequently, the smoothness term gets more priority. When a voxel is on or near the edge of the foreground and the background, we have $(S_A - S_B)^2 \to 0$. Then, following (2.9), we get: $\lambda_x \to \lambda_{max}$. Consequently, the data term gets more importance. In this manner, our probabilistic strategy provides appropriate weights to the data term and the smoothness term, based on the position of a voxel in the image.

2.3.4 Imposition of Shape Prior

A simple geometric shape prior [25] is applied to extract a subgraph $G_1 = G_1(V_1, E_1)$ by pruning the original graph $G = G(V, E)$. As an alternative to more complex methods for shape modeling like Gradient Vector Flow (GVF) snakes [26], the current approach does not need any further user inputs (other than seeds) and has negligible computational overhead. The contour of the skull in the input axial data is

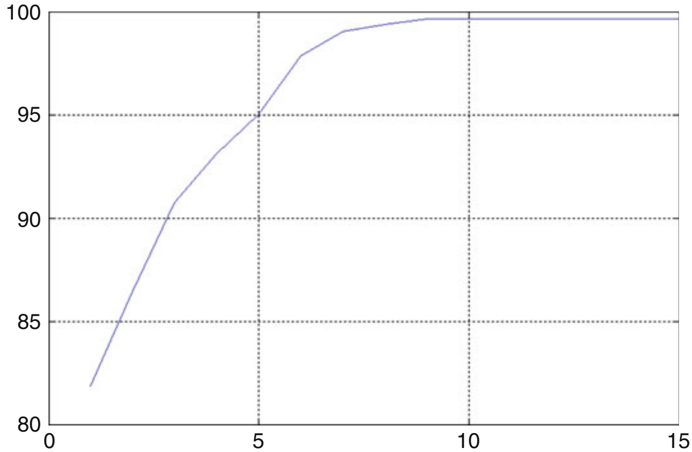

Fig. 2.10 Variation of DC for the probabilistic graph cut algorithm with $K = (K1/K2)$

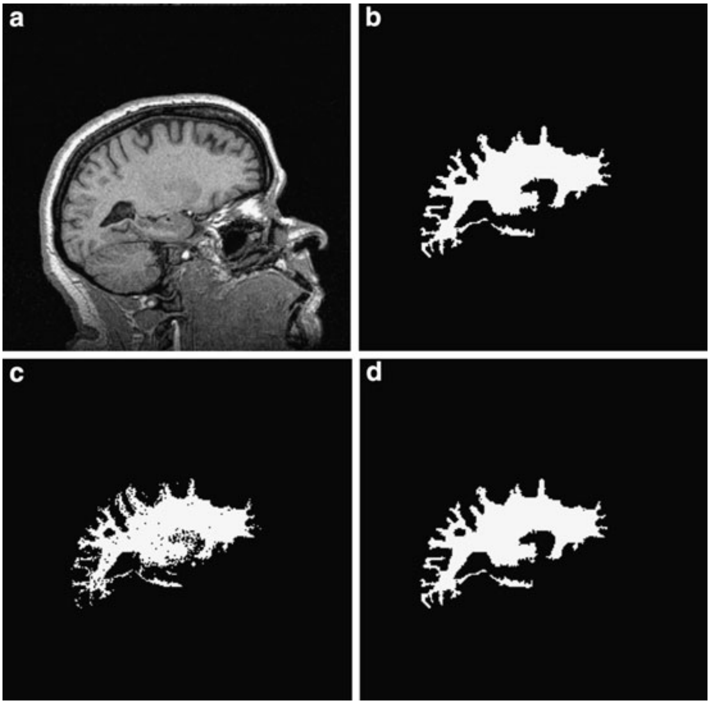

Fig. 2.11 2D Segmentation results from one dataset: (**a**) input, (**b**) ground-truth, (**c**) traditional graph cut (DC = 84.56%), (**d**) probabilistic graph cut (DC = 97.23%)

modeled as an ellipse with center (α, β), semi-major axis a, and semi-minor axis b. The equation for the ellipse is:

$$\frac{(x-\alpha)^2}{a^2}+\frac{(y-\beta)^2}{b^2}=1 \tag{2.13}$$

The contours of the skull appearing in various 2D slices in the input can be appropriately modeled by a series of ellipses. The center of such a typical ellipse in any slice is obtained from the seeds inputted by the user in that particular slice. The other two parameters of the ellipse, namely, a and b are extracted from the image using simple geometry. In this way, we can get the ellipse in only few slices (where the user has provided seeds). For the rest of the slices, bilinear interpolation is employed to obtain the corresponding ellipses. Let $\{p_x(k), p_y(k)\}$ and $\{p_x(m), p_y(m)\}$ respectively denote the coordinates of a pixel p lying on the ellipse in the slice k and that of in the slice m respectively. Then, the coordinates of the pixel p lying on the ellipse in the slice l, where $k < l < m$, are given by:

$$p_x(l)=\frac{(l-k)}{(m-k)}p_x(k)+\frac{(m-l)}{(m-k)}p_x(m) \tag{2.14a}$$

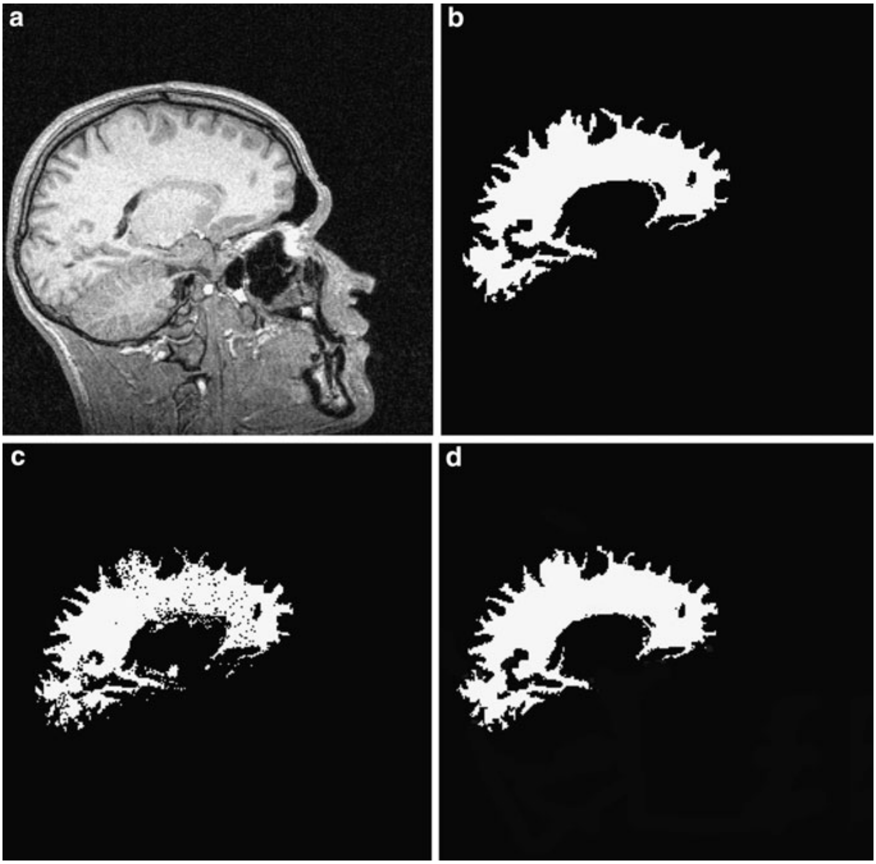

Fig. 2.12 2D Segmentation results from a second dataset: (**a**) input, (**b**) ground-truth, (**c**) traditional graph cut (DC = 87.29%), (**d**) probabilistic graph cut (DC = 96.31%)

$$p_y(l) = \frac{(l-k)}{(m-k)} p_y(k) + \frac{(m-l)}{(m-k)} p_y(m) \tag{2.14b}$$

The potential target voxels lie inside the contour of the skull. Once these target voxels, *i.e.*, the vertices of the newly formed subgraph $(P_1 \subset P)$ are obtained, the t-links (T_1) and the n-links (N_1) are constructed. It is obvious that $T_1 \subset T$ and $N_1 \subset N$. So, we can write $V_1 = P_1 \cup s \cup t$ and $E_1 = T_1 \cup N_1$. The subgraph construction has two distinct advantages. Firstly, the time-complexity of the Ford-Fulkerson algorithm, used to find a minimum cut, is reduced considerably. Note that the augmenting paths are detected using the Edmonds-Karp algorithm [27]. The time-complexity of the Edmonds-Karp method, on the original graph $G = G(V, E)$ is $\mathbf{O}(VE^2)$ and that on the subgraph $G_1 = G_1(V_1, E_1)$ is $\mathbf{O}(V_1 {E_1}^2)$. Let us assume that: $V_1 = \gamma V$ and $E_1 = \delta E$, where γ and δ are two fractions. Let us put $\mu = \gamma\delta^2$. Obviously, the value of $\mu \ll 1$. Now, the time-complexity of the Edmonds-Karp algorithm on the subgraph becomes $\mathbf{O}(\mu VE^2)$; which is $\ll\mathbf{O}(VE^2)$. The second advantage is that the proposed construction has significantly improved the segmentation accuracy as will be shown in the next section.

2.4 Experimental Results

The results reported in this section are based on experimentation with different sets of T1-weighted MRI sequences. We have run our algorithm on both 2D and 3D brain images. For 2D experiments, typically, a single slice (of size 256×256 pixels) is chosen from an entire 3D dataset in a completely unbiased manner while for 3D, we experiment with an entire dataset. The probabilistic graph cut-based segmentation results are compared with the ground-truth as well as with the results obtained from other standard segmentation algorithms like the traditional graph cut and the EMS. The ground-truth has been obtained from manual segmentation done

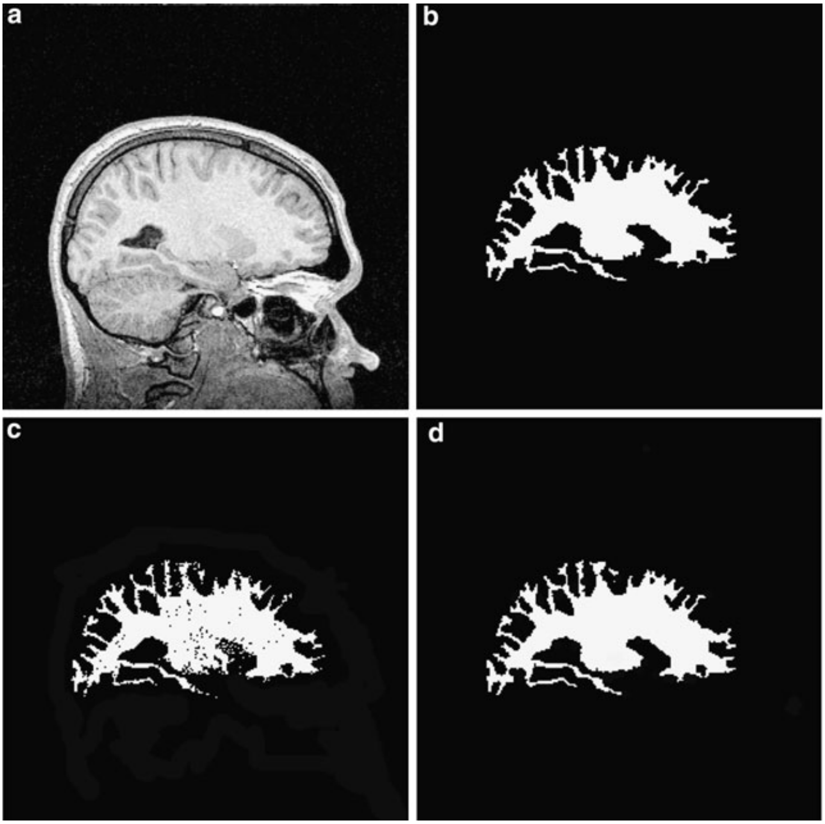

Fig. 2.13 2D Segmentation results from a third dataset: (**a**) input, (**b**) ground-truth, (**c**) traditional graph cut (DC = 90.85%), (**d**) probabilistic graph cut (DC = 97.17%)

by the domain experts. In addition to qualitative comparisons, we also undertake quantitative validations using Dice coefficient. Dice coefficient DC (A, B) between two sets A and B is defined below:

$$\mathrm{DC}(A,B) = 2(|A \cap B|)/(|A| \cup |B|) \tag{2.15}$$

Values of dice coefficients for different segmentation algorithms with respect to the ground-truth are used to judge the relative performances of the different segmentation algorithms.

As a part of the experimental results, we first discuss the choice and estimation of different parameters for both 2D and 3D experiments. The seeds for the probabilistic graph cut algorithm are manually entered in only a few slices for any given dataset. The centers of the ellipses are obtained from the manually entered seeds in these slices using image geometry. For the rest of the slices, the ellipses are generated through bilinear interpolation. Both bilinear and biquadratic interpolations are

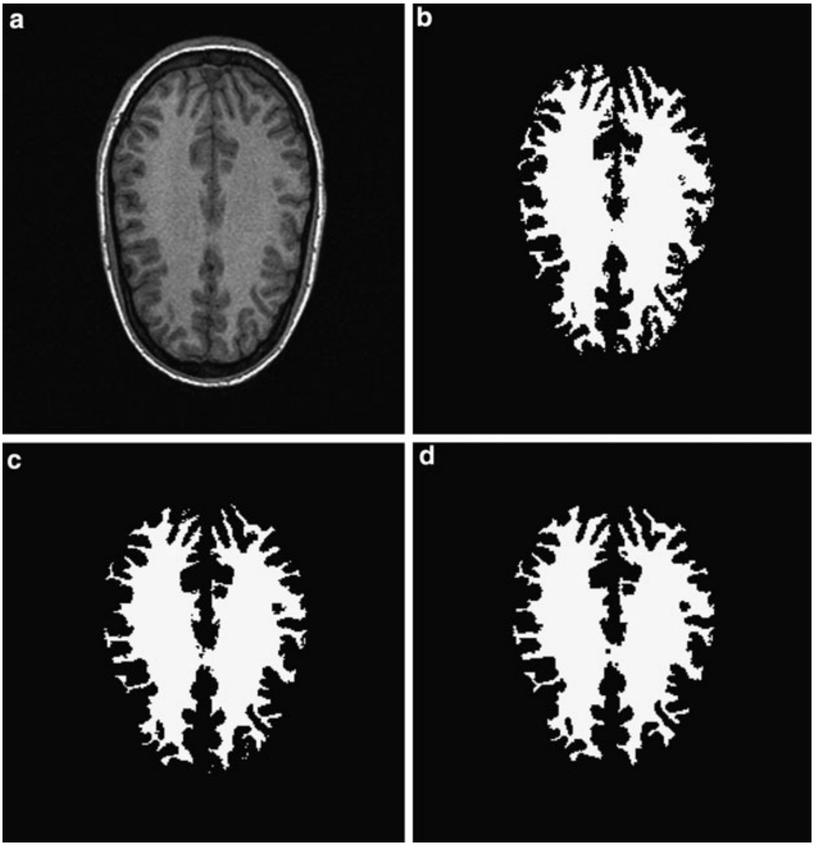

Fig. 2.14 Axial view: (**a**) input, (**b**) graph cut output, (**c**) probabilistic graph cut output, (**d**) ground truth

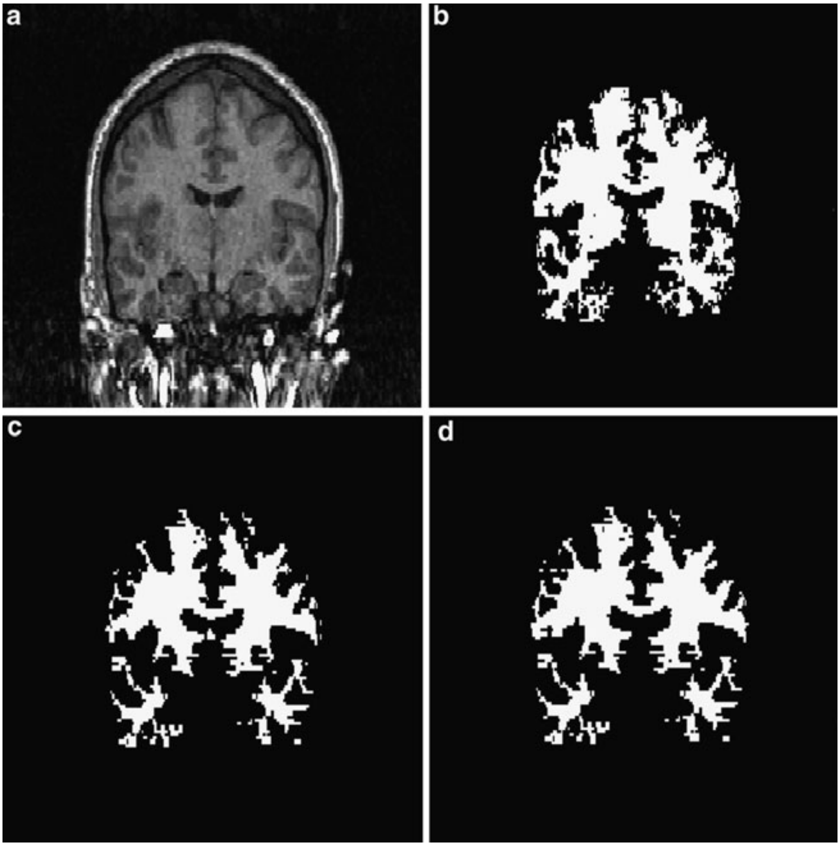

Fig. 2.15 Coronal view: (**a**) input, (**b**) graph cut output, (**c**) probabilistic graph cut output, (**d**) ground truth

employed. No noticeable differences are observed in the results from the above two interpolation techniques. So, we stick to the less complex bilinear interpolation. From the above discussion, it is also evident that very little user input is required in the entire process. The parameter $\lambda_{\max}$ is kept fixed at 70. The value of the parameter σ, which can be treated as "camera noise", is estimated as 3. It is shown in the Sect. 3.2, that for a low-contrast image, there is a lower limit of the parameter K (the ratio of $K1$ and $K2$) above which the accuracy of segmentation is independent of the value of K. If a suitable value of K (above the lower limit) is chosen, then the desired segmentation results can be achieved for the images of same or higher contrast. A plot of Dice coefficient of the probabilistic graph cut algorithm with variation of K for a typical dataset with 5% contrast is shown in Fig. 2.10.

In Figure 2.10, we show that after K has reached a value of 8.7, the value of the Dice coefficient remains almost constant. We fix the value of K at 10 throughout because the other experimental datasets have contrasts greater than or equal to 5%.

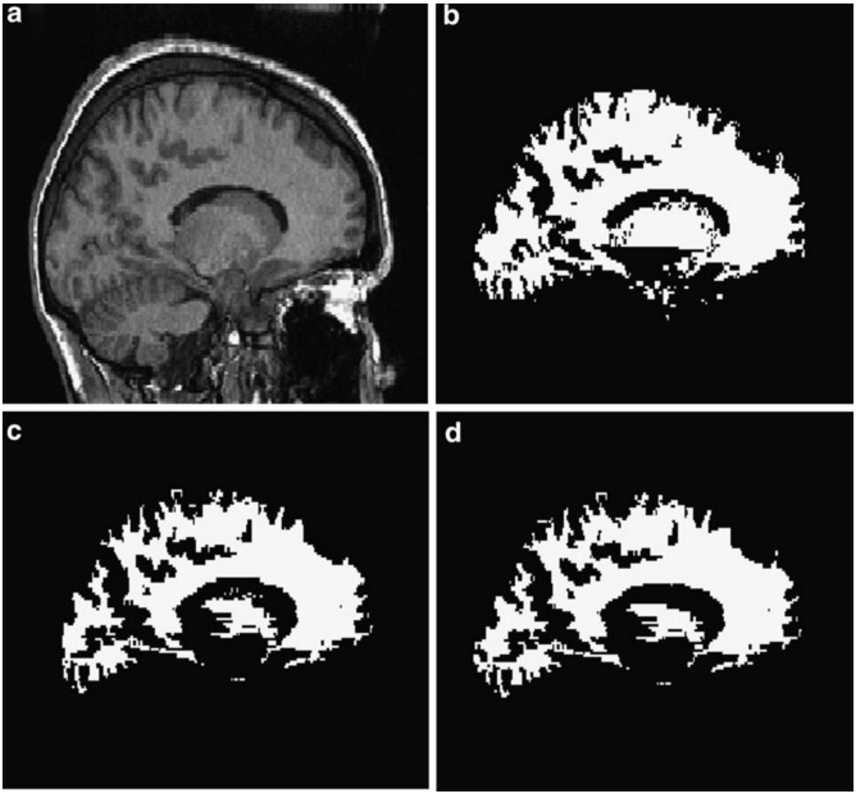

Fig. 2.16 Sagittal view: (**a**) input, (**b**) graph cut output, (**c**) probabilistic graph cut output, (**d**) ground truth

We next present the results of segmentation on three different 2D slices randomly selected from three different datasets. In Figs. 2.11–2.13, we show the outputs of the probabilistic graph cut-based segmentation, the traditional graph cut-based segmentation, and the ground-truth for these 2D slices. The figures clearly demonstrate that the probabilistic graph cut-based segmentation results are much closer in appearance to the respective ground-truths. For example, in Fig. 2.11, DC from the probabilistic graph cut (97.23%) is much higher than DC from the traditional graph cut (84.56%), which indicates superior performance of the probabilistic graph cut algorithm. Similarly, in Fig. 2.12, DC from probabilistic graph cut (96.31%) is once again much higher than DC from traditional graph cut (87.29%) which points to the consistent better performance of the probabilistic graph cut algorithm. Same nature of results is also corroborated by Fig. 2.13.

Now, we show the results of 3D segmentation using probabilistic graph cut algorithm for two MRI sequences. Each 3D sequence contains 124 slices (axial scans) and as mentioned earlier and each slice has dimensions of 256 pixels $\times$ 256 pixels. Three different views, namely, the axial, the coronal, and the sagittal of the

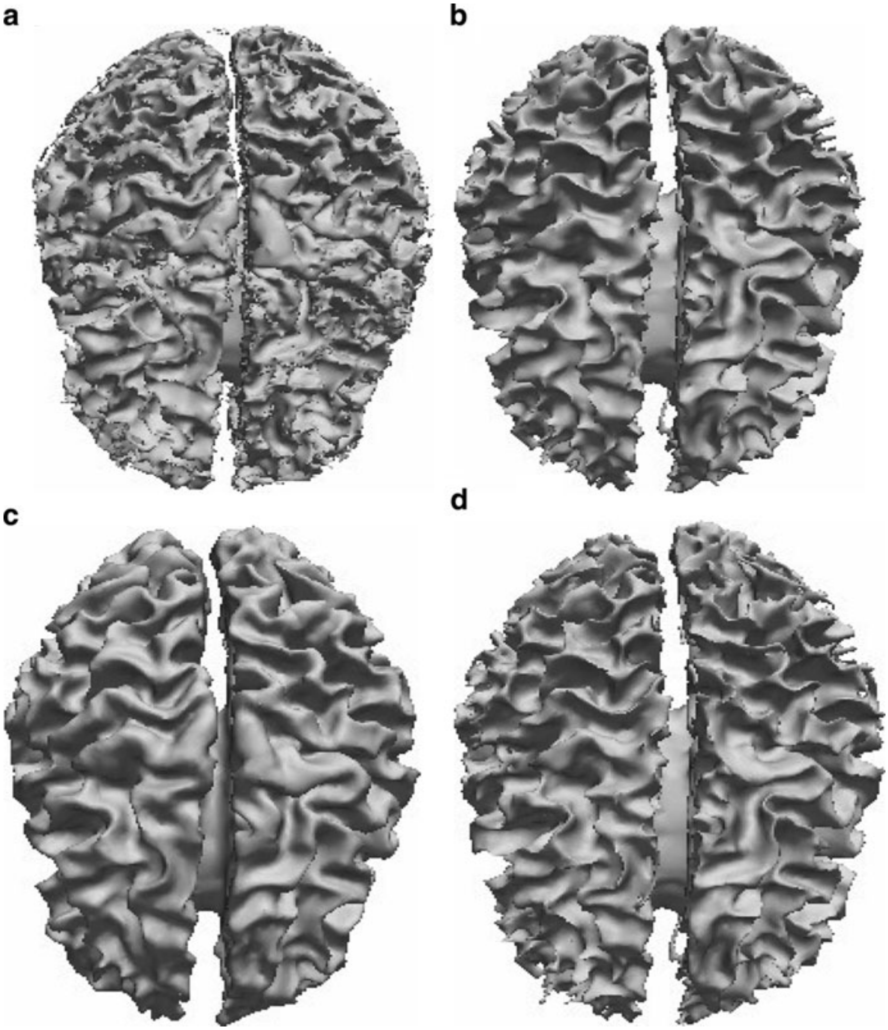

Fig. 2.17 3D Segmented surfaces: (**a**) from graph cut (DC = 88.18%), (**b**) from probabilistic graph cut (DC = 96.99%), (**c**) from EMS (DC = 93.25%), and (**d**) ground truth

same 3D dataset are presented. Figure 2.14 shows the axial view of the input, graph cut-based segmented output, probabilistic graph cut-based segmented output, and ground-truth respectively. Figures 2.15 and 2.16 respectively illustrate the coronal and the sagittal view of the same. In Fig. 2.17, we show the 3D segmented surfaces from the probabilistic graph cut, traditional graph cut, EMS, and ground-truth. The segmented surface from the probabilistic graph cut algorithm bears closest resemblance with the surface obtained from ground-truth. As far as quantitative evaluations are concerned, DC obtained from the probabilistic graph cut (96.99%) is higher than both the traditional graph cut (88.18%) and the EMS (93.25%). In

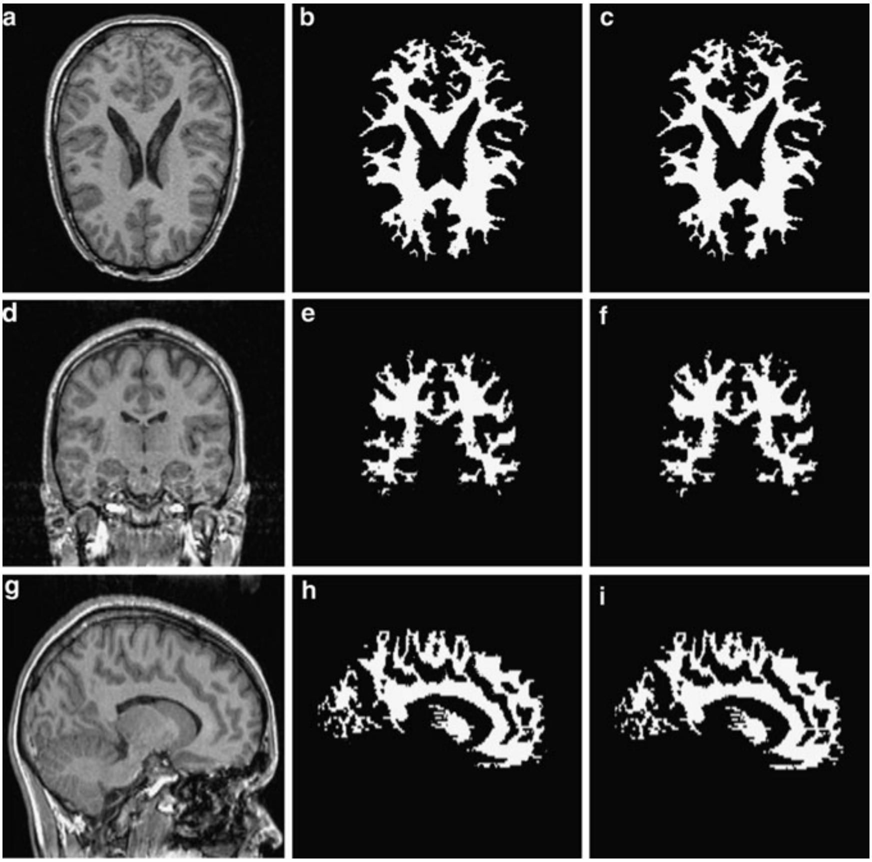

Fig. 2.18 Axial view: (**a**) input, (**b**) probabilistic graph cut output, (**c**) ground truth. Coronal view: (**d**) input, (**e**) probabilistic graph cut output, (**f**) ground truth. Sagittal view: (**g**) input, (**h**) probabilistic graph cut output, (**i**) ground truth

Fig. 2.18, we present the axial, coronal and sagittal views of the input, probabilistic graph cut-based segmented output, and ground-truth of a second 3D dataset. Similarly, in Fig. 2.19, the 3D segmented surfaces from the probabilistic graph cut and the ground-truth are shown.

We end this section with a discussion on the robustness of our proposed method. The proposed method is fairly robust as its performance is found to be quite insensitive to the user inputs. For example, even if the centers of the ellipses are off by few pixels, only a negligible change ($< 0.5\%$) is noticed in the value of the Dice Coefficient. The only basic requirement was that object (white matter in the present case) seeds had to be placed on object and the background seeds had to be placed on the background. In Figs. 2.20 and 2.21, we show two box plots [28] of DC of the traditional graph cut algorithm and that of the probabilistic graph cut algorithm with variations in contrast in the input MRI sequences respectively.

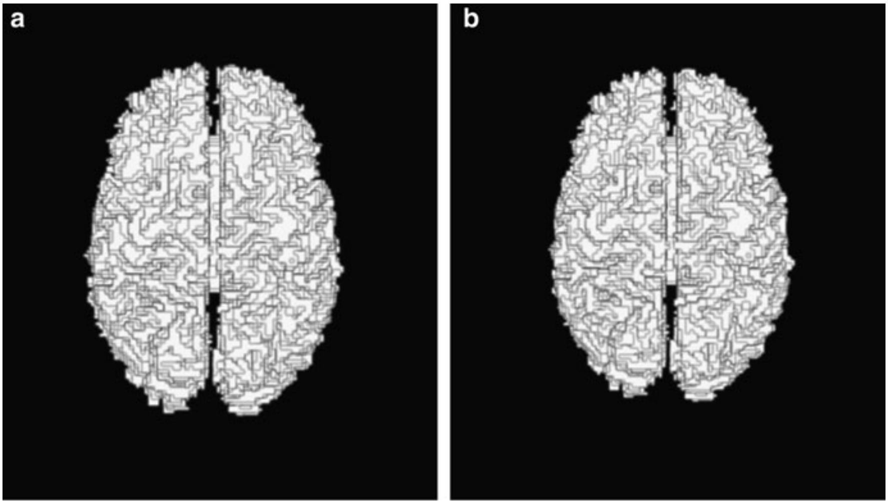

Fig. 2.19 3D Segmented surfaces of another MRI dataset: (**a**) from probabilistic graph cut (DC = 97.12%), (**b**) ground truth

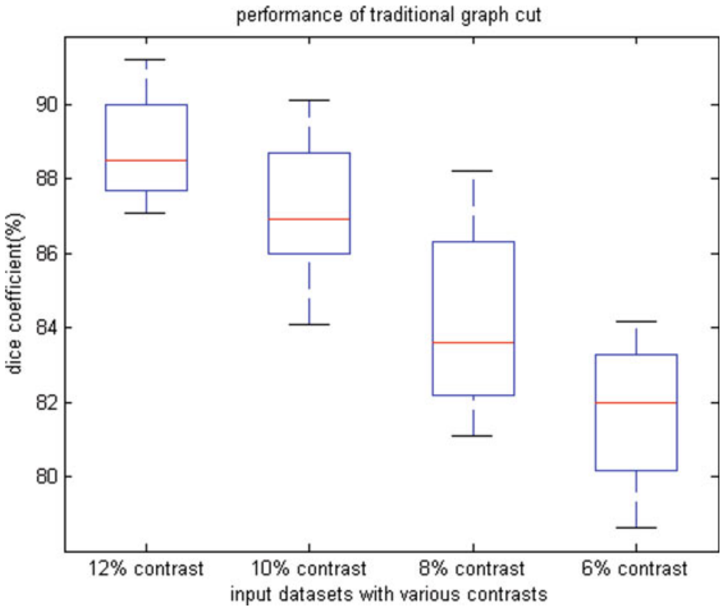

Fig. 2.20 Box plot of performance of the traditional graph cut algorithm with variation in contrast in the input MRI sequences

From Fig. 2.20, it can be easily observed that the mean DC (indicated by the red line) decreases considerably with decrease in contrast in the input datasets. On the other hand, Fig. 2.21 clearly demonstrates that the mean DC reduces only by a little amount

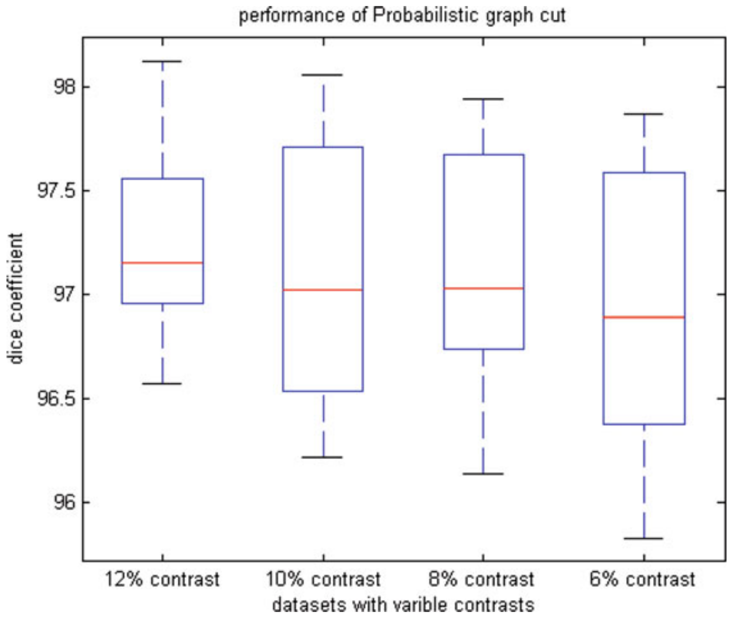

Fig. 2.21 Box plot of performance of the probabilistic graph cut algorithm with variation in contrast in the input MRI sequences

with the same decrease in contrast in the input datasets. Therefore, it can be inferred from these two figures that the probabilistic graph cut outperforms the traditional graph cut, more so for images with low contrasts.

2.5 Conclusion

In this paper, we have addressed the problem of segmentation of cerebral white matter from T1-weighted MRI data. The problem is of great interest to both the computer vision as well as the medical community. The segmentation problem becomes very challenging due to the complicated shape of the white matter and extremely poor contrast between the object and the surrounding structures in the input data. From the medical point of view, accurate segmentation of cerebral white matter will enable us to better understand different neurological disorders. We propose a probabilistic graph cut algorithm, where a probabilistic modification is applied to the traditional graph cut algorithm. We also adopt a probabilistic strategy for estimating the value of the weighting parameter for the smoothness and the data terms for each individual voxel in the input. In addition, we impose a simple yet effective shape prior in form of a series of ellipses to model the human skull in the axial 2D slices constituting an input sequence which increases the speed of execution as well as the accuracy of the segmentation. The method proposed in this paper is extremely fast and has outperformed both the traditional graph cut and the EMS algorithms. More sophisticated techniques like GVF snakes can be explored in conjunction with the proposed probabilistic graph cut algorithm for modeling the human skulls to further improve the segmentation accuracy.

References

1. Levy SE, Mandell DS, Schultz RT (2009) Autism. Lancet 374(9701):1627–1638
2. Warfield SK, Westin CF, Guttman CRG, Albert M, Jolesz FA, Kikinis R (1999) Fractional segmentation of white matter. In: Taylor C, Colchester A (eds) MICCAI 1999. LNCS, vol 1679. Springer-Verlag Berlin Heidelberg, pp 62–72
3. Yang F, Jiang T, Zhu W, Kruggel F (2004) White matter lesion segmentation from volumetric MR images. In: Yang G-Z, Jiang T (eds) MIAR 2004. LNCS, vol 3150. Springer-Verlag Berlin Heidelberg, pp 113–120
4. Boykov Y, Jolly MP (2001) Interactive graph cuts for optimal boundary and region segmentation of objects in N-D images. In: IEEE international conference on computer vision, pp 105–112
5. Boykov Y, Veksler O, Zabih R (2001) Fast approximate energy minimization via graph cuts. IEEE Trans Pattern Anal Mach Intell 23(11):1222–1239
6. Ishikawa H (2003) Exact optimization for Markov random fields with convex priors. IEEE Trans Pattern Anal Mach Intell 25(10):1333–1336
7. Kim J, Zabih R (2003) A segmentation algorithm for contrast-enhanced images. In: IEEE international conference on computer vision, pp 502–509
8. Boykov Y, Funka-Lea G (2006) Graph cuts and efficient N-D image segmentation. Int J Comput Vis 70(2):109–131
9. Van Leemput K, Maes F, Vandermeulen D, Colchester A, Suetens P (2001) Automated segmentation of multiple sclerosis lesions by model outlier detection. IEEE Trans Med Imaging 20(8):677–688
10. Chowdhury AS, Rudra AK, Sen M, Elnakib A, El-Baz A (2010) Cerebral white matter segmentation from MRI using probabilistic graph cuts and geometric shape priors. In: IEEE international conference on image processing, (to appear)
11. Atkins M, Mackiewich B (1998) Fully automatic segmentation of the brain in MRI. IEEE Trans Med Imaging 17(1):98–107
12. Farag A, El-Baz A, Gimel'farb G (2006) Precise segmentation of multi-modal images. IEEE Trans Image Process 15(4):952–968
13. Thacker NA, Jackson A (2001) Mathematical segmentation of grey matter, white matter and cerebral spinal fluid from MR image pairs. Br J Radiol 74:234–242
14. Collins D, Peters T, Dai W, Evans A (1994) Model based segmentation of individual brain structures from MRI data. SPIE Vis Biomed Comput 1808:10–19
15. Kass M, Witkin A, Terzopoulos D (1987) Snakes: active contour models. Int J Comput Vis 1:321–331
16. Caselles V, Kimmel R, Sapiro G (1997) Geodesic active contours. Int J Comput Vis 22:61–79
17. Zeng X, Staib L, Duncan J (1998) Volumetric layer segmentation using coupled surface propagation. In: IEEE international conference on computer vision pattern recognition, pp 708–715
18. Wolz R, Aljabar P, Rueckert D, Heckemann AR, Hammers A (2009) Segmentation of subcortical structures in brain MRI using graph-cuts and subject-specific a-priori information. In: IEEE international symposium on biomedical imaging, pp 470–473
19. Peng B, Veksler O (2008) Parameter selection for graph cut based image segmentation. In: British machine vision conference, pp 1–10

20. Freedman D, Zhang T (2005) Interactive graph cut based segmentation with shape priors. In: IEEE international conference on computer vision, pp 755–762
21. Song Z, Tustison N, Avants B, Gee J (2006): Adaptive graph cuts with tissue priors for brain MRI segmentation. In: IEEE international symposium on biomedical imaging, pp 762–765
22. Zhang J, Wang Y, Shi X (2009) An improved graph cut segmentation method for cervical lymph nodes on sonograms and its relationship with node's shape assessment. Comput Med Imaging Graph 33:602–607
23. Ford LR, Fulkerson DR (1962) Flows in networks. Princeton University Press, Princeton, NJ
24. Kolomogorov V, Zabih R (2004) What energy functions can be minimized via graph cuts. IEEE Trans Pattern Anal Mach Intell 26(2):147–159
25. Slabaugh G, Unal G (2005) Graph cuts segmentation using an elliptical shape prior. In: IEEE international conference on image processing, pp 1222–1225
26. Xu C, Prince JL (1998) Snakes, shapes and gradient vector flow. IEEE Trans Image Process 7(3):359–369
27. Cormen TH, Leiserson CE, Rivest RL, Stein C (2001) Introduction to algorithms. MIT Press, Cambridge, MA
28. Tukey JW (1977) Exploratory data analysis. Addison-Wesley, Reading, MA

Biography

Mainak Sen passed his 12th standard from Ramakrishna Mission Vivekananda Centenary College, West Bengal in 2007. He is currently an undergraduate student of Bachelor in Engineering (B.E.) in Department of Electronics and Telecommunication Engineering., Jadavpur University, India. He worked as research assistant in Department of Computing Science, University of Alberta, Canada. His research interest includes computer vision, pattern recognition, and biomedical image processing.

Ashish Kumar Rudra got his 12th standard degree from Krishnanagar Collegiate School, West Bengal in 2007. Now, he is a 4th year student of Bachelor in Engineering (B.E.) in Department of Electronics and Telecommunication Engineering, Jadavpur University, India. He worked as research assistant in CIMS Lab, Department of Computing Science, University of Alberta, Canada. His research interest includes computer vision, pattern recognition and biomedical image processing. He is also interested in abstract algebra, literatures recitation and painting.

Ananda S Chowdhury received a B.Sc. (Hons.) in Physics from Presidency College, Calcutta, India in 1996, a B.Tech. in Electronics Engineering from the Institute of Radiophysics and Electronics, Calcutta, India in 1999, and an M.E. in Computer Engineering from Jadavpur University, Calcutta, India in 2001. He earned his Ph.D. in Computer Science at the University of Georgia, Athens, Georgia in July 2007. From July 2007 to December 2008, he was as a postdoctoral fellow in Radiology and Imaging Sciences at the National Institutes of Health, Bethesda, Maryland. At present, he is working as a Reader in the Electronics and Telecommunication Engineering department of Jadavpur University, Calcutta, India.

Ahmed Elnakib received his B.Sc. and M.Sc. degrees in Electronics and Communication Engineering from Mansoura University, Egypt, in 2003 and 2007, respectively. Mr. Elnakib joined the BioImaging Laboratory as research assistance in September 2008. His current research includes developing new computer assisted diagnosis systems, image modeling, image segmentation, 2-D and 3-D registration, and shape analysis of detected lung nodules.

Ayman El-Baz received the B.Sc. and M.S. degrees in electrical engineering from Mansoura University, Egypt, in 1997 and 2000, respectively and the Ph.D. degree in electrical engineering from University of Louisville, Louisville, KY. He joined the Bioengineering Department, University of Louisville, in August 2006. His current research is focused on developing new computer-assisted diagnosis systems for different diseases and brain disorders

Springer

http://www.springer.com/978-1-4419-8203-2

Multi Modality State-of-the-Art Medical Image
Segmentation and Registration Methodologies
Volume II
El-Baz, A.S.; Acharya U, R.; Laine, A.F.; Suri, J. (Eds.)
2011, X, 368 p., Hardcover
ISBN: 978-1-4419-8203-2